Materials Chemistry and Physics 287 (2022) 126152

Contents lists available at ScienceDirect

Materials Chemistry and Physics

journal homepage: www.elsevier.com/locate/matchemphys

Experimental and computational investigation of 3,5-di-*tert*-butyl-2-(((3-((2-morpholinoethyl)(pyridin-2-ylmethyl) amino) propyl)imino) methyl)phenol and related reduced form as an inhibitor for C-steel

Saeid Karimi [a,**], Majid Rezaeivala [b,*], Koray Sayin [c], Burak Tuzun [c]

[a] Department of Metallurgy and Materials Engineering, Hamedan University of Technology, Hamedan, 6516913733, Iran
[b] Department of Chemical Engineering, Hamedan University of Technology, Hamedan, 6516913733, Iran
[c] Sivas Cumhuriyet University, Faculty of Science, Department of Chemistry, 58140, Sivas, Turkey

HIGHLIGHTS

- Two inhibitors containing morpholine tags have been synthesized and characterized.
- The corrosion studies show an excellent corrosion inhibitor of two ligands.
- Scanning electron microscopy evaluations confirm the protection of carbon steel.
- The adsorption mechanisms preferred the Langmuir adsorption isotherm.
- Molecular modeling provides more information into the inhibition performance.

GRAPHICAL ABSTRACT

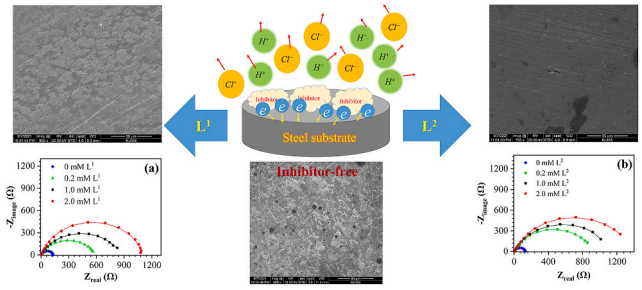

ARTICLE INFO

Keywords:
Schiff base
Morpholine
Acid corrosion
EIS
Electrochemistry
Acid inhibition
C-Steel
Modeling studies

ABSTRACT

The effect of new compounds containing morpholine moiety including: *3,5-di-tert-butyl-2-(((3-((2-morpholinoethyl)(pyridine-2-ylmethyl)amino)propyl)imino)methyl)phenol (L^1)* and its reduced form, *3,5-di-tert-butyl-2-(((3-((2-morpholinoethyl)(pyridine-2-ylmethyl)amino)propyl)amino) methyl)phenol (L^2)* on the corrosion inhibiting of C-steel in 1.0 M HCl and 3.5 wt% NaCl was tested by experimental and computational techniques. The concentration of inhibitor varied in the range of 0.2–2.0 mM. The corrosion behavior of C-steel was investigated using electrochemical techniques, including open circuit potential (OCP), potentiodynamic polarization (Tafel), electrochemical impedance spectroscopy (EIS) and scanning electron microscopy (SEM) inhibitor-free and inhibitor-containing solutions. From the Tafel diagram, the i_{corr} of the C-steel electrode in the 1.0 M hydrochloric acid solution represents the highest value among the other inhibitor-containing solutions. The i_{corr} for C-steel in L^1 containing solution decreases gradually from 1.43×10^{-4} to 0.91×10^{-4} A/cm^2, with the concentration of L^1 increasing from 0.2 to 2.0 mM. Along with the increase of the L^2 concentration from 0.2 to 2.0 mM, the i_{corr} is reduced by about 41%. EIS studies demonstrated that the capacitance of the double layer increased by the addition of inhibitors and increasing the resistance of charge transfer, suggesting an improvement of the corrosion protection in inhibitor-containing acidic solution. SEM images confirmed the corrosion results in which

* Corresponding author.
** Corresponding author.
E-mail addresses: s.karimi@hut.ac.ir (S. Karimi), mrezaeivala@hut.ac.ir (M. Rezaeivala).

https://doi.org/10.1016/j.matchemphys.2022.126152
Received 19 August 2021; Received in revised form 21 March 2022; Accepted 16 April 2022
Available online 19 April 2022

inhibitor-containing solution protects the C-steel surface against the attack of species. The results showed that in all solutions containing equivalent concentrations of inhibitors, the reduced form of L^1 had a better inhibition efficiency than the L^1 inhibitor. Inhibitors, L^1 and its reduced form exhibit Langmuir adsorption isotherm, in which monolayer adsorption of inhibitors is carried out on the C-steel electrode. The properties of the studied molecules to be corrosion inhibitors were examined with the Gaussian software program. The calculations of the molecules were made in different methods and basis sets.

1. Introduction

A broad range of organic inhibitors applied in the corrosion domain is expensive [1]. Electron pairs and negative ions are transferred from the inhibitors to the metal d orbitals, resulting in coordination complexes with specific geometries [1]. It is well-known that the coupling between an aldehyde and amine can be readily carried out and that the produced imine compound undergoes hydrolysis under acidic conditions [2]. These compounds have attracted significant and increasing interest in various aspects [3]. There are many studies, as well as some of ours on the synthesis of various Schiff base ligands containing piperazine and morpholine moieties [4–7]. Also, there are some reports on the application of imines for metal corrosion prevention [8–11]. There is a desire to use iron alloys in the industry due to the low cost and high strength in different applications.

Meanwhile, carbon-containing iron alloys (i.e., steel) play a significant role in various industrial sections, including constructions of building and railway, gas and oil industry, etc. [12]. Since C-steel alloys are used in common aqueous environments, the corrosion behavior of these types of alloys seems to be very important for the management of corrosion costs [13]. There are two main strategies to improve the corrosion rate and elongate the life of C-steel in harsh acidic media, including the use of highly resistant alloys in corrosion media and the addition of organic inhibitor compounds in the acidic solutions [14]. The availability and low cost of organic inhibitors result in extensive usage in acidic solutions [15–17]. Recently, the potential of corrosion protection of inhibitors containing imines [18], azines [19], sulphonamides [20], thiols [21], etc. has been investigated in the literature. Generally, organic inhibitors contain O, N, P and S heteroatoms which show inhibiting behavior in acidic media [12,22]. The protection mechanism of inhibitors can be explained by the adsorption of organic atoms on the steel surface and then filling the surface of the particles and removing corrosive ions from the C-steel surface [15]. Although there are many common inhibitors in the industries, numerous efforts are being made to introduce new groups of organic inhibitors to increase the inhibition efficiency and minimize the corrosion costs [23]. Therefore, there is a serious need to research this field and introduce new materials to achieve the mentioned aims.

Barmatov and Hughes [24] stated that most of the inhibitors used in sulfuric acid and hydrochloric acid solutions have insufficient hydrolytic stability at low pH conditions. Only a few studies have been performed to investigate the corrosion resistance of reduced forms of inhibitors [15,

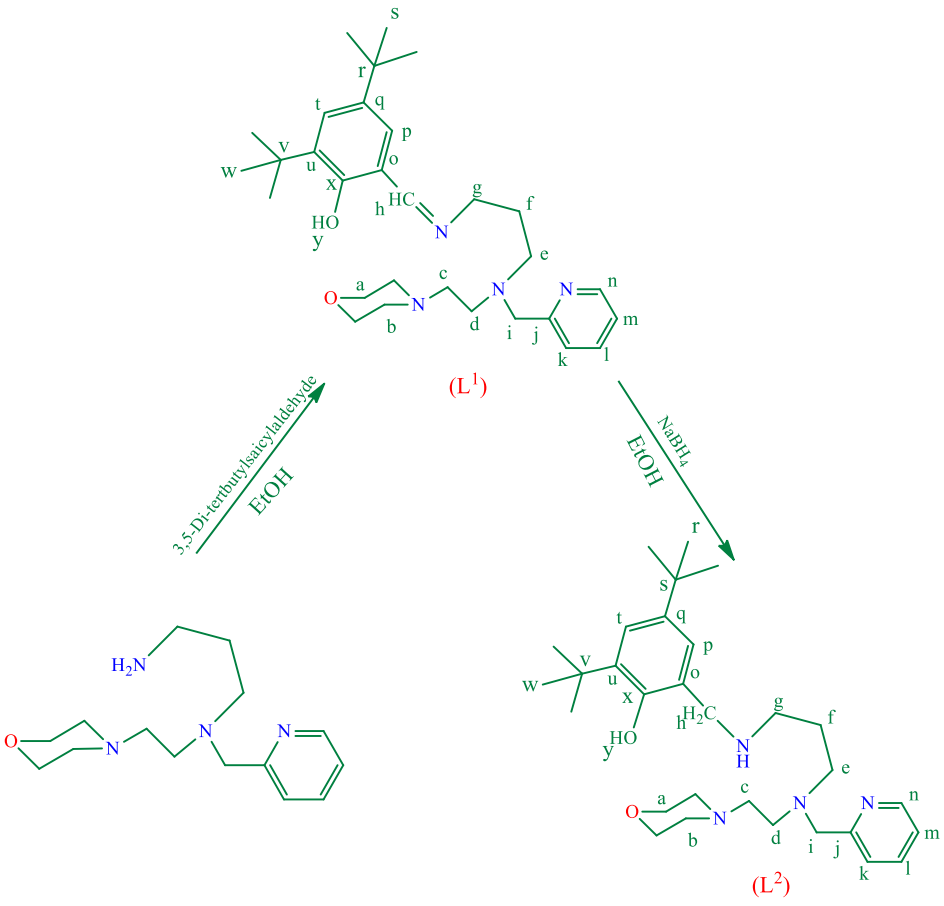

Scheme 1. Synthesis of L^1 and L^2.

24–26].

Here, the main goal is to investigate the behavior of L^1 and its reduced form as an inhibitor on C-steel corrosion in a 1.0 M hydrochloric acid solution by using electrochemical impedance measurements (EIS). Theoretical calculations are a better guide than experimental procedures. With the quantum chemical parameters found as a consequence of theoretical calculations, the inhibitory properties of molecules are expected to be predicted. This process is faster and more accessible [27]. The calculations of the molecules were made in different methods and basis sets and afterward, the comparison of the inhibition properties of the inhibitor molecules with the obtained parameters was made.

2. Experimental

N1-(2-morpholinoethyl)-N1-((pyridine-2-yl)methyl)propane-1,3-diamine and 3,5-di-*tert*-butyl-2-hydroxy benzaldehyde were synthesized according to literature methods [6,27,28]. Pyridine-2-carbaldehyde and 2-aminoethylmorpholine were purchased from Sigma Aldrich Company. IR spectra were collected on a BIO-RAD FTS-40A spectrophotometer (4000-400 cm^{-1}). Nuclear NMR spectra were recorded on a Bruker 500 spectrometer operating at 500.06 MHz, respectively. Mass spectra were measured on a Bruker micro TOFQ. Standard microanalysis for all complexes was carried out using a CHNS/O elemental analyzer (model 2400, Perkin-Elmer).

2.1. Synthesis

2.1.1. Synthesis of 3,5-di-tert-butyl-2-(((3-((2-morpholinoethyl)(pyridin-2-ylmethyl) amino)propyl)imino)methyl)phenol (L^1)

An ethanolic solution *of N1-(2-morpholinoethyl)-N1-((pyridine-2-yl) methyl)propane-1,3-diamine* (0.5 mmol, 0.139 g) was added dropwise to the stirring solution of *3,5-di-tert-butyl-2-hydroxy benzaldehyde* (0.5 mmol, 0.117 g) in ethanol (50 mL). The mixture was refluxed for 12 h. A brown oil was obtained that was filtered off, washed with cold ethanol and dried in vacuo. Yield: (85%). Anal. Calc. for $C_{30}H_{46}N_4O$: C, 75.27; H, 9.69; N, 11.70. Found: C, 75.00; H, 9.83; N, 11.22%. IR (ATR, cm^{-1}): 3424, 1633 υ(C═N), 1590, 1470 υ(C═C). EI-MS (*m/z*): 494.710, Found: 494.500 $[L]^+$. ^1H NMR ($CDCl_3$, ppm) $\delta = 1.32$ (s, 9H, H-r); 1.43 (s, 9H, H-w); 1.88 (p, 2H, H-f); 2.40 (t, 4H, H-b); 2.49 (t, 2H, H-e); 2.69 (t, 4H, H-c, H-d); 3.61 (t, 2H, H-g); 3.68 (t, 4H, H-a); 3.79 (s, 2H, H-i); 7.06 (d, 1H, H-k); 7.10 (t, 1H, H-m); 7.47 (t, 1H, H-s); 7.49 (s, 1H, H-p); 7.61 (t, 1H, H-l); 8.31 (s, 1H, H-h); 8.51 (d, 1H, H-n); 13.81 (s, 1H, H-y). ^{13}C NMR ($CDCl_3$, ppm) $\delta = 29.28$ (c-r); 29.43 (c-s); 31.32 (c-v); 31.52 (c-w); 28.46 (c-f); 51.47 (c-c); 52.08 (c-d); 54.08 (c-b); 56.99 (c-e); 57.16 (c-g); 60.94 (c-i); 66.91 (c-a); 117.80 (c-m); 121.85 (c-o); 122.83 (c-p); 125.67 (c-k); 126.68 (c-t); 127.84 (c-u); 131.85 (c-l); 136.33 (c-q); 148.91 (c-n); 157.80 (c-x); 160.14 (c-h); 165.96 (c-j) (Scheme 1).

2.1.2. Synthesis of 3,5-di-tert-butyl-2-(((3-((2-morpholinoethyl)(pyridin-2-ylmethyl)amino)propyl)amino) methyl)phenol (L^2)

To an ethanlic solution (50 mL) of *2-((3-(2-morpholinoethylamino)-N3-((pyridine-2-yl)methyl) propylimino) methyl)pyridine* (0.5 mmol, 0.239 g) was added slowly sodium borohydride (0.25 mmol, 0.009 g). The mixture was refluxed for 12 h. A brown oil was obtained that was filtered off, washed with cold ethanol and dried in vacuo. Yield: (85%). Anal. Calc. for $C_{30}H_{48}N_4O$: C, 74.95; H, 10.06; N, 11.65. Found: C, 75.03; H, 9.89; N, 11.92%. $^{-1}$ IR (ATR, cm): 3232 $\upsilon(N–H)_{str}$, 1675 $\upsilon(N–H)_{bend}$, 1591 υ(C═N), 1479 υ(C═C). EI-MS (*m/z*): 496.73, Found: 497.50 $[L+1]^+$. ^1H NMR ($CDCl_3$, ppm) $\delta = 1.33$ (s, 9H, H-s); 1.43 (s, 9H, H-r); 1.75 (p, 2H, H-f); 2.38 (t, 4H, H-b); 2.43 (t, 4H, H-c); 2.49 (t, 2H, H-d); 2.62 (t, 2H, H-e); 2.75 (t, 2H, H-g); 3.63 (t, 4H, H-a); 3.75 (s, 2H, H-h); 3.93 (s, 2H, H-i); 6.79 (d, 1H, H-k); 6.88 (t, 2H, H-m); 7.12 (s, 1H, H-p); 7.24 (t, 1H, H-l); 7.29 (s, 1H, H-t); 8.45 (d, 1H, H-n). ^{13}C NMR ($CDCl_3$, ppm) $\delta = 29.67$ (c-r); 29.72 (c-s); 30.06 (c-f); 31.72 (c-v); 31.80 (c-w); 34.13 (c-g); 34.90 (c-h); 45.96 (c-c); 47.19 (c-d); 51.10 (c-h); 54.03 (c-b); 56.84 (c-e); 60.73 (c-i); 66.82 (c-a); 122.02 (c-m); 122.98 (c-o); 136.37 (c-k); 148.88 (c-t); 148.96 (c-u); 153.41 (c-n); 154.75 (c-j); 157.96 (c-l); 153.41 (c-n); 159.70(c-x) (Scheme 1).

Table 1
Chemical composition (in wt. %) of the base metal.

Elements	C	Si	Ni	Mn	P	Cr
wt. %	0.049	0.010	0.003	0.221	0.013	0.001

2.2. Immersion time measurements

The weight loss measurements were performed using coupons with a dimension of $1 \times 1 \times 0.1$ cm^3 cuts from the C-steel. The electrodes were polished with emery papers, followed by rinsing with acetone and ethanol and dried in hot air and kept in a desiccator. The C-steel samples were immersed in 50 ml of 1.0 M HCl solution (inhibitor-free) and different concentrations of inhibitors (0–2 mM) for 12 h. These experiments were done at a temperature of 22 °C. After every 1 h, the samples were taken out and rinsed several times with deionized water and acetone. Next, they were dried in an oven and then weighed. The experiments were repeated at least twice under similar conditions, and the average result was recorded.

2.3. Calculation method

Calculations were made using the Gaussian software program [29] to compare the theoretical activities of inhibitor molecules. Inhibitor molecules were optimized by these calculations. Many quantum chemical parameters were obtained in calculations using these optimized structures. For the optimization of molecules, calculations were made on the B3lyp, HF, and M062X method 6–31++g(d, p) basis set. Many quantum chemical parameters were calculated as a result of the calculations made on these basis sets. Many quantum chemical parameters have been calculated from these calculations. These are EHOMO (Highest Occupied Molecular Orbital), ELUMO (Lowest Unoccupied Molecular Orbital), ΔE (HOMO-LUMO energy gap), electronegativity (χ), chemical potential (μ), chemical hardness (η), electrophilicity (ω), nucleophilicity (ε), global softness (σ) and proton affinity (PA) [30,31].

2.4. Solutions, electrodes and electrochemical experiments

Electrochemical measurement was carried out with a conventional three-electrode-electrochemical cell using a Potentiostat/galvanostat set (Iviumstat compact 20250 H) controlled by IviumSoft electrochemistry software and a GSTAT101 N Potentiostat (Metrohm Autolab) controlled by Nova software (Version 2.1.4). The C-steel was used as the working electrode, and its chemical composition is shown in Table 1. An Ag/AgCl electrode (Metrohm) filled with 3.5 M KCl (217 mV vs. SHE at 22 °C) and a platinum electrode was employed as a reference and counter electrodes, respectively. Before electrochemical testing, C-steel was mounted by epoxy cold resin to have a surface area of 1 cm^2 exposed to the corrosive solution. The electrodes were ground wet to 1500 grit SiC followed by rinsing with acetone and ethanol and dried in hot air. 1.0 M hydrochloric acid and 3.5 wt % NaCl solutions were used as electrolyte for all electrochemical experiments. The electrochemical experiments were carried out under non-stirred, ambient pressure, and a controlled temperature of 22 °C. Two new substances, including L^1 and L^2 forms, were used to compare the inhibitors' results. The concentration of inhibitors was varied within the range of 0.2–2.0 mM.

To ensure the accuracy of analyses, experiments were started only after stabilizing the open circuit potential (OCP) within ±5 mV [32]. For the Tafel tests, the current values were recorded in the range ±0.70 V vs. OCP at a constant scan rate of 10 mV/s and converted to current density by figuring the surface area. Electrochemical impedance spectroscopy (EIS) tests were conducted in 100 ml of a 1.0 M HCl solution with and without inhibitors at OCP. The frequency range was 10^{-1}–10^5 Hz with

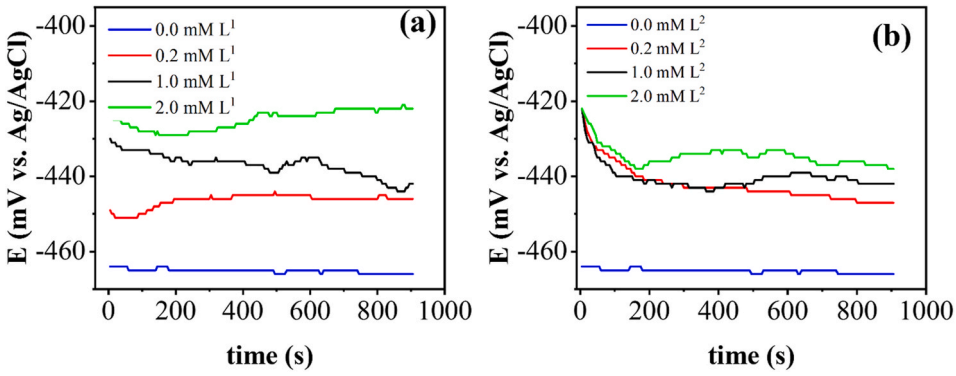

Fig. 1. The OCP value of C-steel in 1.0 M HCl at different concentrations of (a) L^1 and (b) L^2.

peak–to–peak amplitude of 10 mV. Each electrochemical experiment was repeated at least twice to ensure the reproducibility of results.

2.5. Surface characterization

The C-steel surface of the sample was characterized by an FEI Quanta 450 scanning electron microscope (SEM), which was equipped with energy-dispersive X-ray spectroscopy (EDS). The C-Steel was cut into 1 × 1 × 1 cm^3, and then the surface of the samples was polished on emery paper of 400, 800, 1000 and 1500 grades. The polished surface was washed twice with distilled water and ultrapure acetone, respectively. Subsequently, the specimens were immersed in 100 ml of 1.0 M HCl solution with and without L^1 and L^2 inhibitors for 24 h. Finally, the samples were rinsed with distilled water and acetone to remove any adhered particles.

3. Result and discussion

3.1. Characterization of L^1 and L^2

A new Schiff base ligand (L^1) was prepared through the condensation reaction of *N1-(2-morpholinoethyl)-N1-((pyridine-2-yl)methyl)propane-1,3-diamine* and *3,5-di-tert-butyl-2-hydroxy benzaldehyde*, with a molar ratio of 1:1, for 6 h in ethanol. The prepared ligand and related reduced form were characterized by microanalysis and some spectroscopic techniques.

3.1.1. FT-IR and mass spectra

The FT-IR spectrum of the L^1 showed a sharp band at 1633 cm^{-1} related to the stretching vibration frequency of the imine group, indicating the condensation of the precursors to produce the Schiff base ligand. The mass spectrum of the L^1 showed the molecular ion peak at m/z = 494.71amu, which is consistent with the proposed molecular formula. The L^2 was prepared by an in-situ reduction of the Schiff-base ligand and characterized by microanalysis, IR, EI-MS and ^1H and ^{13}C NMR spectroscopy. The IR spectrum of L^2 showed bands at 1591, 1570 and 1479 cm^{-1}, associated with the υ(C═N) and υ(C═C) vibrations from the pyridine ring. The υ(N–H) bending and stretching bands appeared at 1675 and 3232 cm^{-1}, respectively. The mass spectrum of L^2 showed the molecular ion peak at m/z = 497.50 seen to be consistent with the proposed molecular formula.

3.1.2. NMR spectral studies

The ^1H and ^{13}C NMR spectra of ligands (L^1 and L^2) were recorded in $CDCl_3$. The peaks obtained were consistent with the structures of the synthesized Schiff base and its reduced compound. For both compounds, the aromatic protons appeared as multiples between 7.06 and 8.51 ppm. The imino proton, for L^1, was observed at 8.31 ppm, while in the reduced form, the singlet at δ 3.75, due to $–CH_2$- group, confirmed the formation of the L^2. The ^{13}C NMR spectrum showed the signals due to the methyl carbon at 51.10 ppm, and the peaks which appeared in the range 122.02–159.70 ppm reflected the aromatic carbons. The peak due to the imino carbon in L^1 appeared at 160.14 ppm.

3.2. Electrochemical measurements in 1.0 M HCl

3.2.1. OCP measurements

The OCP magnitude for samples can be precisely a sign of their electrochemical activity. The OCP evolution of the C-steel in 1.0 M HCl solution in the absence and presence of different concentrations of L^1 and L^2 is shown in Fig. 1. After immersion of the C-steel electrode in inhibitor-free solution (1.0 M HCl), the OCP was almost unchanged during its measurement for 900 s. The OCP of the C-steel generally reached a steady-state condition in the first 200 s after being immersed in test solutions. More evident in Fig. 1a, the C-steel OCP in the L^1-containing solutions showed a higher value than the L^1-free solution. The reaching OCP value for C-steel in the L^1-containing solution occurs in the early stage of immersion in 1.0 M HCl (c.a. 200 s), as is clear from Fig. 1a. During the first 200 s, the OCP value varied around 6 mV for the C-steel in the L^1 solution. After that OCP value fluctuated in a small range (less than 5 mV), which can be assigned to the competitive dynamic process by desorption and adsorption of the inhibitor on the C-steel surface [33,34]. The OCP value gradually increases from −446 to −422 mV vs. Ag/AgCl by increasing the L^1 concentration in the range of 0.2–2.0 mM. The positive shift of the OCP can be attributed to the terms of the adsorption of inhibitor molecules on the C-steel layer [35]. It is supposed that the anodic reactions like iron oxidation in the presence of inhibitors can retard under OCP conditions [36]. These results confirm that a higher concentration of L^1 promotes the inhibition efficiency of samples in a 1.0 M HCl solution.

While the OCP variation with time follows from Fig. 1b that the addition of inhibitor L^2 to the 1.0 M hydrochloric acid solution generates new characteristics in the OCP curve. The OCP value for C-steel in three different concentrations of inhibitor L^2 (e.g. 0.2, 1.0 and 2.0 mM) initially decreases from c.a. −420 mV Ag/AgCl to a minimum value of −440 mV vs. Ag/AgCl for 200 s and then stabilizes. These findings could be explained by the inhibition of the cathodic reaction on the C-steel surface for the first 200 s after electrode immersion into 1.0 M HCl solution. It is evident that the slow increase in OCP value at a concentration of 1.0 mM and 2.0 mM of L^2 inhibitor may be attributed to the anodic reaction being inhibited after 200 s [37]. Similar to the L^1-containing solution, the OCP of the C-steel in the L^2-containing solutions show a positive shift compared with the inhibitor-free solution. This positive shift in the value of the OCP was discovered to enhance with an increase in the concentration of L^2. The maximum change in OCP was found to be 26 mV at a concentration of 2.0 mM for inhibitor L^2. The OCP of the C-steel in the L^2-containing solutions is in the potential range of −445 to −437 mV vs. Ag/AgCl, which shows a narrow potential range

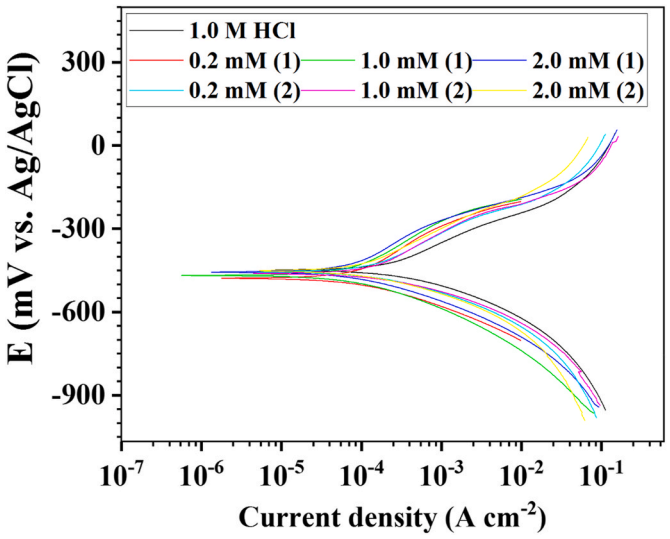

Fig. 2. Tafel diagram for C-steel in 1.0 M HCl solution in the absence and various concentration inhibitors of L^1 and L^2.

compared to the L^1-containing solutions. Like the result of the L^1, a 1.0 M HCl solution containing L^2 has a higher OCP compared to L^2-free solution. The increase in OCP values by the addition of L^1 and L^2 inhibitors as compared to inhibitor-free demonstrates the importance of inhibition performance, which helps to protect the C-steel surface from the corrosion process.

3.2.2. Potentiodynamic polarization

Tafel diagram, as presented in Fig. 2, can be used to determine electrochemical parameters, including the corrosion current density, i_{corr}, and corrosion potential of C-steel (E_{corr}). Additionally, the cathodic coefficients (β_c) and the apparent anodic coefficients (β_a) are calculated by the aid of the slopes of the Tafel diagram and Tafel equations, as follows:

$$\log i_{ox} = \log i + \frac{\alpha_a n F E_{corr}}{2.3RT} \quad (1)$$

$$\log i_{red} = \log i - \frac{\alpha_c n F E_{corr}}{2.3RT} \quad (2)$$

where i_{red} and i_{ox} are the reduction and oxidation current densities, while n, F, T, and R demonstrate the number of transferred electrons, faradaic constant, absolute temperature (K), and ideal gas constant, respectively. The Tafel curves of the C-steel in the absence and presence of inhibitors revealed similar polarization diagrams, implying no considerable difference in the polarization result between the inhibitor-free and inhibitor-containing solutions.

The i_{corr} for C-steel is precisely the evidence of its corrosion damage. As a result, an electrode with a higher i_{corr} will corrode faster than a lower i_{corr} at fixed E_{corr} [38,39]. As shown in Table 2, the i_{corr} of the C-steel electrode in 1.0 M HCl solution is 2.33×10^{-4} A/cm^2 representing the highest value among the other inhibitor-containing solutions. The i_{corr} for C-steel in the L^1-containing solution decreases gradually from 1.43×10^{-4} to 0.91×10^{-4} A/cm^2 by raising the concentration of L^1 from 0.2 to 2.0 mM. Table 2 shows that the L^1 has lower i_{corr} compared to L^2 at all concentrations, which could be due to the polarized functional groups of C═O and the NH_2 with better adsorbing capability on the steel surface compared to the CH_2–NH group of lower polarity in L^2. It is seen that the addition of the reduced form of L^1 in the 1.0 M HCl solution provided a superior result with the best resistance to corrosion as compared to the L^1-free and containing solutions. Along with the increase of the L^2 concentration from 0.2 to 2.0 mM, the i_{corr} is reduced by about 41%. A similar conclusion can be drawn by using the results of corrosion rate, in which the C-steel showed a higher corrosion resistance in the L^2-containing solution in comparison to the inhibitor-free and L^1-containing solutions. By Assessing Table 2, resistance polarization (R_P) of the C-steel in the free-inhibitor solution is the lowest one (108.73 Ω cm^2) compared with the C-steel in inhibitor-containing solutions. It is again confirmed the lowest corrosion resistance among the other samples. The more concentration of inhibitors L^1 and L^2 leads to the high values of R_p. In addition, the inhibitor L^2 shows higher R_p than that L^1 in the equal concentration, indicating the higher corrosion performance C-steel in the L^2-containing solution.

From Table 2, at all solutions (except inhibitor-free solution), β_a is greater than β_c. If β_a is greater than β_c, the double layer formed on the electrode surface shows the p-type semiconductor behavior [40]. Therefore, the double layer formed on the C-steel surface in inhibitor-containing solutions acts as p-type semiconductor behavior. Generally, both apparent charge transfer coefficients decrease by increasing the concentration of inhibitors. In addition, it is reported that a reduced form of the inhibitor has higher stability hydrolytically in hydrochloric acid media because the reduced amine does not endure the hydrolytic process [15,24]. In this study, the imine bond (−C═N−) is converted to an amine bond (−C–NH) by the reduction process.

By assessing the obtained data, the change in E_{corr} between the C-steel electrode in the presence inhibitor with respect to the blank 1.0 M HCl was less than 20 mV for all concentrations. Previously published stated if the difference in E_{corr} was less than 85 mV, the inhibition mechanism could be recognized as a mixed-type, showing that the process rate of anodic inhibition was nearly equal to the cathodic reactions [41,42]. However, based on the OCP and Tafel polarization measurements for the C-steel in the absence and presence of inhibitors, it is believed that L^1 and L^2 act as mixed a mixed type system with anodic inhibition predominant.

3.2.3. EIS study

The simulated and measured Nyquist impedance spectra of C-steel at the OCP in the absence and presence of inhibitors, L^1 and L^2, are shown in Fig. 3a and b. Only one time constant can be seen in the testing frequency range for the samples in 1.0 M HCl with and without inhibitors, which is generally attributed to a process that mainly corresponds to a charge transfer phenomenon on the electrode surface. The Nyquist diagram obtained in different concentrations of L^1 and L^2 is attributed to the capacitive impedance of a double−layer with a charge transfer resistance on the surface of the C-steel electrode. It is worth mentioning that the shape of Nyquist diagrams is a depressed semi-circle and accommodates the non-ideal behavior of a capacitance. This phenomenon

Table 2
Tafel diagram data for C-steel in 1.0 M HCl solution in the absence and various concentration inhibitors of L^1 and L^2.

Sample	Conc. (mM)	$E_{corr.}$ (mV)	$i_{corr.}$ (A/cm^2)	β_a (V/dec)	$-\beta_c$ (V/dec)	$-\beta_a/\beta_c$	R_P (Ω.cm^2)
1.0 M HCl	0	−448.80	2.33×10^{-4}	0.111	0.123	0.90	108.73
L^1	0.2	−449.75	1.43×10^{-4}	0.130	0.097	1.34	168.68
	1.0	−445.07	1.24×10^{-4}	0.140	0.096	1.45	199.42
	2.0	−446.37	0.91×10^{-4}	0.130	0.113	1.15	288.46
L^2	0.2	−464.11	1.25×10^{-4}	0.160	0.106	1.51	221.48
	1.0	−464.07	0.88×10^{-4}	0.149	0.087	1.71	271.03
	2.0	−464.73	0.74×10^{-4}	0.139	0.093	1.49	326.95

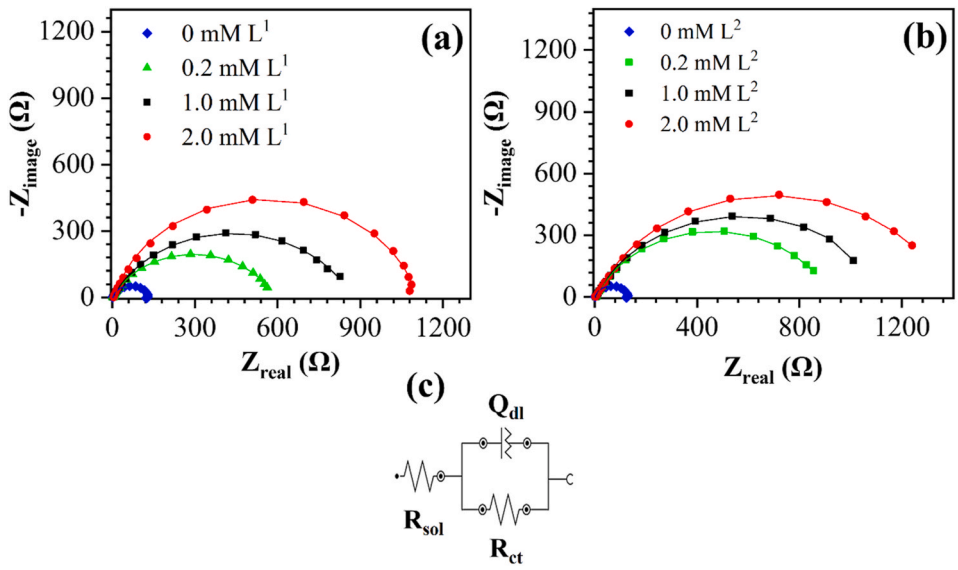

Fig. 3. Simulated and measured Nyquist impedance spectra of C-steel at OCP in 1.0 M HCl at different concentrations of (a) L^1 and (b) L^2, and (c) an equivalent circuit on the electrode surface.

Table 3
EIS parameters for an equivalent circuit of Fig. 3c

Inhibitor type	Concentration (mM)	$R_{sol.}$ (Ω cm^2)	R_{ct} (Ω cm^2)	Q_{dl}		χ^2
				Y_0 (Ω s^{-n})	n	
1.0 M HCl	0.0	2.41	126.06	1.31×10^{-4}	0.89	0.013
L^1	0.2	2.41	585.60	1.35×10^{-4}	0.75	0.001
	1.0	2.00	868.21	1.18×10^{-4}	0.75	0.009
	2.0	2.98	1098.00	1.07×10^{-4}	0.76	0.006
L^2	0.2	7.19	912.20	1.08×10^{-4}	0.78	0.004
	1.0	4.94	1136.10	1.01×10^{-4}	0.77	0.008
	2.0	6.73	1379.40	1.00×10^{-4}	0.75	0.002

illustrates using constant phase element (CPE), which includes two electrochemical parameters; Y_0 (the admittance of CPE) and n (empirical constant). The value below 1.0 arises from the roughness of the C-steel surface and inhomogeneity owing to the inhibitors adsorption together with the corrosion products [8].

In addition, an equivalent electrical circuit is depicted in Fig. 3c and its electrochemical parameters are shown in Table 3. An equivalent electrical circuit designed to fit EIS diagrams, contains a resistance of 1.0 M HCl solution ($R_{sol.}$) in series with Q_{dl}/R_{ct}. As already known, charge transfer resistance is a characteristic quantity for corrosion resistance; the higher the charge transfer resistance, the higher the corrosion resistance. From charge transfer resistance values given in Table 3, the resistance obtained in the presence of L^1 was quite higher than that in the absence of L^1 (126.06 Ω cm^2). Also, the trend for the inhibition efficiency for L^1 follows the order of 2.0 mM > 1.0 mM > 0.2 mM. The charge transfer resistance for C-steel in the L^1-containing solution increases significantly from 585.6 to 1098.0 Ω cm^2 by promoting the concentration of L^1 from 0.2 to 2.0 mM. It is apparent in Table 3 that with increasing the L^2 concentration, an increment in the value of R_{ct} is observed (912.20–1379.40 Ω cm^2). As a result, the EIS data for inhibitors confirms that the L^2-containing solutions have much better corrosion resistance of the C-steel than the L^1 compound.

The obtained results in EIS measurements are in good accordance with the Tafel experiments. Compared to EIS and Tafel data, the polarization resistance of C-steel in inhibitor-free solution demonstrates the minimum value. While, the R_{ct} and R_P values for inhibitor L^1 and L^2 rise meaningfully in the range of 0.2–2.0 mM in 1.0 M HCl solution, confirming the improvement of the inhibition performance at higher concentration. The charge transfer resistance observed for L^1 and L^2 was similar to that observed in Tafel experiments, so as to C-steel electrode in the L^2-containing solution demonstrates higher R_{ct} than that L^1 in the equal concentration. It is clear that both EIS and Tafel experiment confirm that L^2 inhibitor has higher corrosion resistance at a maximum concentration (2.0 mM), thanks to its higher R_p and R_{ct} makes its use when the environment is too corrosive and aggressive. A similar view has been reported previously that the higher concentration of inhibitors causes the higher charge transfer resistance for metal electrodes [38,43,44].

Generally, an increase in inhibitor concentration leads to an increment in the thickness and surface coverage inhibitor in the steel surface, which effectively adsorbed on the electrode surface [39]. On the other hand, the inhibitor molecules replace water ions on the C-steel surface [45]. Based on the FTIR results, the other reason for this phenomenon can be their inherent feature in that N-containing functional groups play as electron donors to the electrode surface [16]. The existence of hetero elements and aromatic rings such as nitrogen and sulfur on the structure of amino acids causes a weighty increment in inhibition efficiency [46].

The lower capacitance of the double-layer can be evidence of the higher efficiency of the inhibitor performance. The value of the double-layer capacitance is calculated by the following equation [47]:

$$C_{dl} = \left(\frac{Y_0}{R_{ct}^{n-1}}\right)^{\frac{1}{n}} \quad (3)$$

where C_{dl} is capacitive of double layer, Y_0 represents the value of CPE, R_{ct} is the charge transfer resistance, and n is the phase exponent which is always in the range of 0–1. As the following equation, C_{dl} is conversely related to the thickness of the double layer, which serves as a barrier layer for protection from corrosion.

Table 4
The capacitance of double layer and inhibition efficiency values of C-steel in 1.0 M HCl solution containing different concentrations of inhibitors.

Inhibitor type	Inhibitor-free	L^1			L^2		
	1.0 M HCl	0.2 mM	1.0 mM	2.0 mM	0.2 mM	1.0 mM	2.0 mM
C_{dl} (μF cm^{-2})	79.0	57.94	55.21	54.41	56.18	52.17	51.67
IE (%)	–	78.47	85.48	88.51	86.18	88.90	90.86

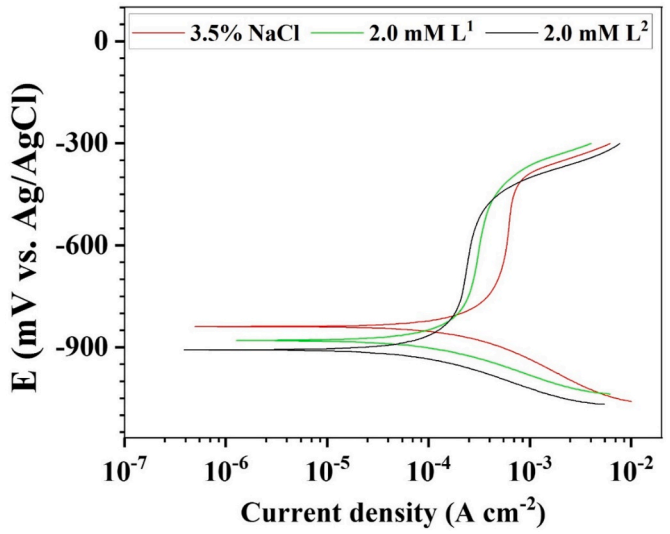

Fig. 4. Tafel diagram data for C-steel in 3.5% NaCl solution in the absence and presence of 2.0 mM inhibitors of L^1 and L^2.

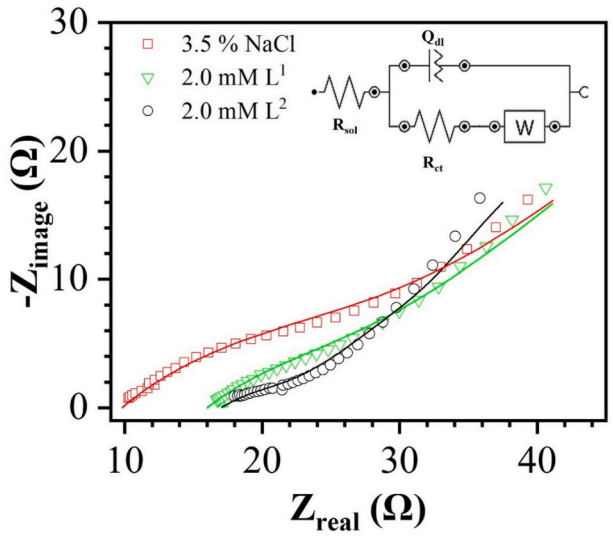

Fig. 5. Nyquist impedance spectra and equivalent circuit of C-steel electrode at OCP in 3.5% NaCl solution in the absence and presence of 2.0 mM inhibitors of L^1 and L^2.

$$C_{dl} = \frac{\varepsilon \varepsilon_0 A}{d} \quad (4)$$

where d is the thickness of the electrical double layer, ε_0 is vacuum permittivity, ε is dielectric constant, and A is the electrode area in the electrolyte. It is clear from the data in Table 3 that an increase in L^1 concentration leads to a gradual decrease in the value of double-layer capacitance (57.94–54.41 μF cm^{-2}), which implies a reduction in dielectric constant or/and increase in the double layer thickness [8]. This phenomenon reflects that the L^1 inhibitors' presence led to the decrement in the capacitance of the double-layer due to the replacement of H_2O molecules by inhibitor ions at the surface of the C-steel electrode. As a result of the inhibitors adsorption on the electrode surface, the effective value of the area (A), which can intensify the corrosion rate, decreases, and the efficiency of surface protection is increased. The adsorption of L^1 molecules on the electrode surface acts as a barrier for ions and charge transfers between metal and electrolyte, thus enhancing the protecting surface from corrosion. These findings confirm the data obtained in EIS analysis, in which higher charge transfer resistance led to higher protection efficiency while the C_{dl} for C-steel in the L^2-containing solutions decreases from 56.18 to 51.67 μF cm^{-2} with increasing the inhibitor concentration, which demonstrates lower C_{dl} values than the L^1-containing solutions. Therefore, C-steel shows high corrosion resistance in the L^2-containing solutions compared to the L^1.

Table 4 also shows the inhibition efficiency (IE) calculated from charge transfer resistance values obtained in EIS diagrams shown in Fig. 3 as follows:

$$IE(\%) = \frac{R_{ct} - R_{ct}^0}{R_{ct}} \times 100 \quad (5)$$

where R_{ct} and R_{ct}^0 present the charge transfer resistance of C-steel with and without inhibitors, respectively. The IE increased by adding more L^1-inhibitor with a maximum IE of 88.51% at 2.0 mM concentration. As shown in Table 4, there is a gradual increment in the inhibition efficiency of the L^1-containing solution from 78.47% to 88.51%, which represents only a 10.04% improvement in corrosion protection by increasing inhibitor concentration from 0.2 mM to 2 mM (tenfold increase in inhibitor concentration). As shown in Table 4, the IE obtained in the presence of L^2 is far greater than the values obtained in the L^1-containing solution. Again, these results suggested that the L^1 is hydrolyzed by HCl into its precursor molecules, C═O and the NH_2 with higher polarity has better absorbance onto the steel surface which increases the C_{dl} value and is slightly higher than the L^2 with lower polarity and adsorbing capability.

3.3. Electrochemical measurements in 3.5 wt % NaCl

Fig. 4 shows Tafel diagram data for C-steel in 3.5% NaCl solution in the absence and presence of 2.0 mM inhibitors of L^1 and L^2. The corrosion parameters including i_{corr}, E_{corr}, β_a and β_c and R_p were measured from the Tafel curves shown in Table 5. The E_{corr} of C-steel in the free-inhibitor solution (3.5% NaCl) was −871.03 mV vs. Ag/AgCl

Table 5
Tafel diagram data for C-steel in 3.5 wt % NaCl in the absence and presence of 2.0 mM inhibitors of L^1 and L^2.

Sample	$E_{corr.}$ (mV)	$i_{corr.}$ (A/cm^2)	β_a (V/dec)	$-\beta_c$ (V/dec)	$-\beta_a/\beta_c$	R_P (Ω.cm^2)
3.5% NaCl	−871.03	3.89×10^{-4}	0.017	0.375	0.046	18.45
2.0 mM L^1	−910.15	1.78×10^{-4}	0.053	0.630	0.084	119.14
2.0 mM L^2	−935.34	1.25×10^{-4}	0.039	0.539	0.072	126.70

Table 6
EIS parameters for an equivalent circuit of Fig. 5

Sample	R_s ($\Omega.cm^2$)	R_{ct} ($\Omega.cm^2$)	Q_{dl}		W ($\Omega.s^{-0.5}$)	χ^2
			Y_0 ($\Omega.s^{-n}$)	n		
3.5% NaCl	9.8	26.3	0.099	0.47	1.9	0.025
2.0 mM L^1	16.1	43.2	0.140	0.45	1.4	0.023
2.0 mM L^2	17.2	51.5	0.110	0.38	1.1	0.015

which is more positive than C-steel in containing-inhibitor solutions. Like the inhibition mechanism of L^1 and L^2 in 1.0 M HCl, the mixed-type mechanism controls the inhibiting process on the C-steel surface in 3.5% NaCl solution, due to the E_{corr} difference being lower than 85 mV [41, 42]. It is fair to say that the inhibition mechanism in C-steel is similar in both 1.0 M HCl and 3.5% NaCl solutions. From Table 5, the i_{corr} of C-steel in 3.5% NaCl was 3.89×10^{-4}, the highest one compared with 2.0 mM L^1 and L^2-containing. As C-steel showed the highest corrosion resistance in 1.0 M HCl solution, the same trend can be seen for C-steel in NaCl solution, in which the i_{corr} for inhibitor L^2 illustrated by 67.9% and 29.8% reduction in corrosion rate compared with the absence inhibitor and 2.0 mM L^1. Moreover, a big difference between the potentiodynamic curve of C-steel in 1.0 M HCl and 3.5%NaCl is the formation of a passive region in sodium chloride solution. At the range −750 to −450 mV vs. Ag/AgCl, in the anodic branch, corrosion rate directly enters the passive region by increasing the applied potential, indicating a hydroxide iron formation on the C-steel surface in contact with the solution [48]. Again, resistance polarization (R_P) of the C-steel in the free-inhibitor solution showed the lowest one (18.45 Ω cm^2) compared with the C-steel in inhibitor-containing solutions. In contrast to the results of the 1.0 M HCl solution, at all solutions, β_a is lower than β_c.

Fig. 5 shows the Nyquist impedance spectra and equivalent circuit of C-steel electrode at OCP in 3.5% NaCl solution in the absence and presence of 2.0 mM inhibitors of L^1 and L^2. As shown in Fig. 5, all Nyquist shows a depressed circle at high frequency and a straight line at low-frequency range, indicating a completely different corrosion mechanism compared with C-steel in 1.0 M HCl. The first semi-circle is generally related to the charge transfer phenomenon. The second part corresponds to the diffusion process through the iron hydroxide layer (passive film) on the surface [49].

Moreover, the Nyquist plots were simulated by an equivalent circuit as shown in Fig. 5 and their electrochemical were demonstrated in Table 6. The circuit consists of a solution resistance (R_s) in series with a parallel capacitive loop charge transfer resistance and capacitance (R_{cl}/Q_{cl}) and a parallel Warburg element. From R_{ct} values given in Table 6, C-steel showed the lowest value (26.3 Ω cm^2). On the other hand, the trend for the inhibition efficiency for C-steel follows the order of 2.0 mM L^2 > 2.0 mM L^1 > inhibitor-free. Therefore, maximum inhibition efficiency can be found in the L^2-containing solution for C-steel. Similar to EIS results in HCl, it can be said that the L^2-containing solutions have much better corrosion resistance for the C-steel than that of the L^1 compounds. The EIS results are in good agreement with the Tafel data in 3.5% NaCl solution. The Warburg element in the equivalent circuit is related to the diffusion process through passive films, which acts as a barrier in mass

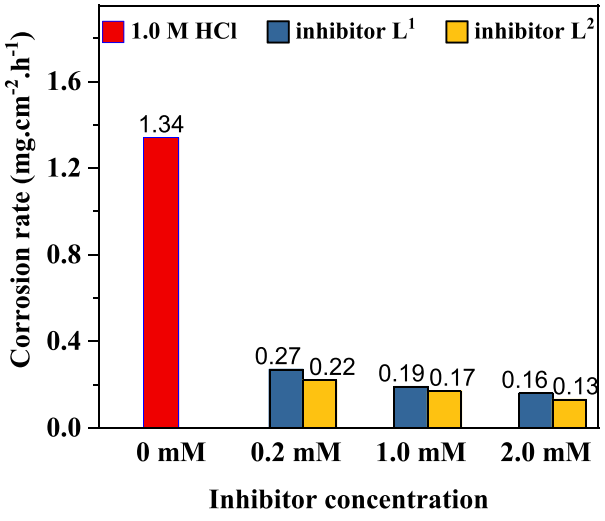

Fig. 6. Corrosion rate of C-steel in the absence and presence of inhibitor L^1 and L^2 solution measured by weight loss experiments.

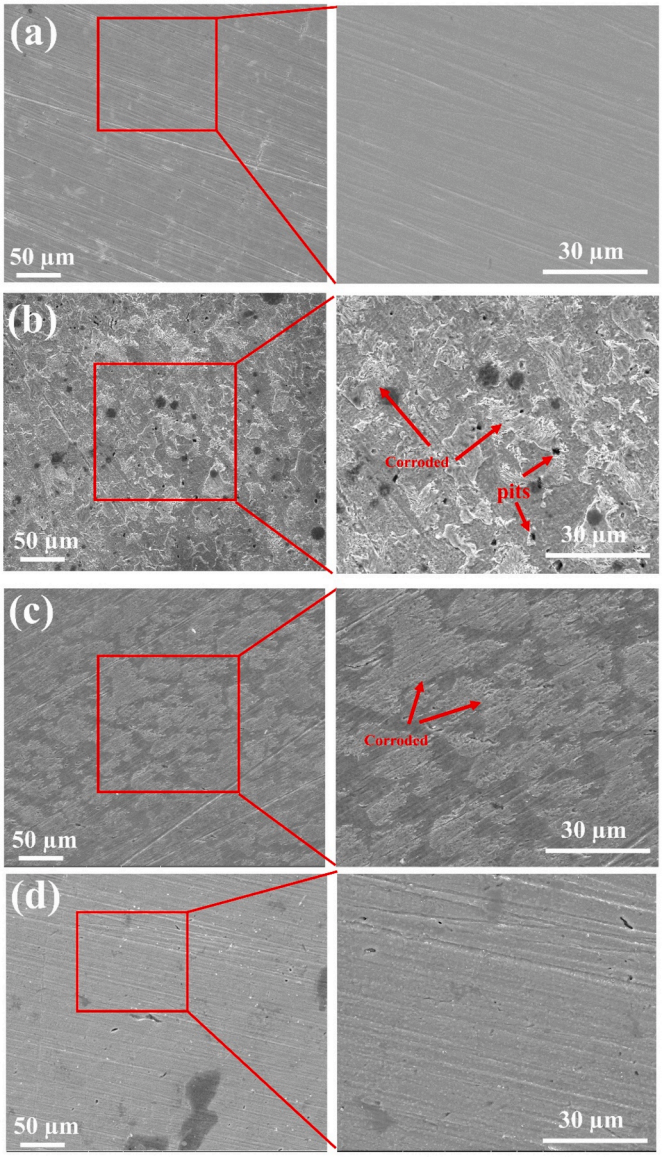

Fig. 7. (a) SEM image of the as-received C-steel surface, and SEM image of C-steel taken after immersion in (b) 1.0 M HCl (inhibitor-free), (c) 2 mM inhibitor L^1 and (d) 2 mM inhibitor L^2.

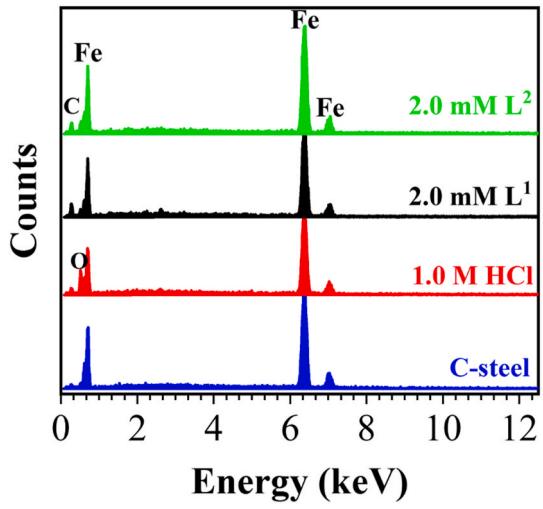

Fig. 8. EDS analysis of the as-received C-steel before dipping in the electrolyte, and after immersion in 1.0 M HCl (inhibitor-free), 2.0 mM inhibitor L^1 and (d) 2.0 mM inhibitor L^2.

transfer. A lower value of Warburg indicates a barrier effect of the passive film slowing down the diffusion of corrosive ions [50]. The Warburg values increased with decreasing inhibition efficiency due to the greater aggressive corrosion agent diffusing through the passive film. Such an increase can be observed for C-steel in free-inhibitor 3.5% NaCl solution.

3.4. Immersion time measurements

The weight loss measurement was used to determine the corrosion rate of C-steel in 1.0 M HCl solution in the absence and presence of inhibitors L^1 and L^2 (as depicted in Fig. 6). It is a way to confirm the obtained data from electrochemical measurements on a time scale as well as the stability of inhibitors. The corrosion rate for C-steel in inhibitor-free solution shows the highest value compared with samples in inhibitor-containing solutions. The obtained data from the immersion test for the sample in 1.0 M HCl is well accordance with our finding in Tafel and EIS measurements, indicating a minimum corrosion resistance for the inhibitor-free solution. As illustrated in Fig. 6, the addition of both inhibitors L^1 and L^2 cause a dramatic decrease in the corrosion rate of C-steel in 1.0 M HCl solution, indicating the improvement in corrosion behavior even a long time. In addition, the corrosion rate decreases gradually from 0.27 to 0.16 mg cm^{-2} h^{-1} for inhibitor L^1 and from 0.22 to 0.13 mg cm^{-2} h^{-1} for inhibitor L^2. Similar results have been reported by previous studies [43,51]. It is fair to say that all corrosion rate data have confirmed the EIS and Tafel polarization experiments at different concentrations of inhibitors.

3.5. Surface characterization

SEM images in Fig. 7 show the corrosion inhibition efficiency of the inhibitors L^1 and L^2 on the C-steel surfaces exposed in 1.0 M HCl. Fig. 7a shows the as-received C-steel before dipping in the electrolyte, which depicts a smooth and clear surface. In an inhibitor-free solution, the surface severely deteriorated at the end of the 24 -hour immersion in 1.0 M HCl, which was confirmed by irregular and rough surface (Fig. 7b). As the inhibitors L^1 and L^2 add to the 1.0 M HCl solution, the corrosion degree of the C-steel surface is decreased which is shown in Fig. 7c and d. This confirmed that the inhibitor-containing solution protects the C-steel surface against corrosive species. It is apparent that the reduced form of L^1 in the 1.0 M HCl solution provided better protection as compared to the L^1-containing solution, confirming a relatively smoother and cleaner surface.

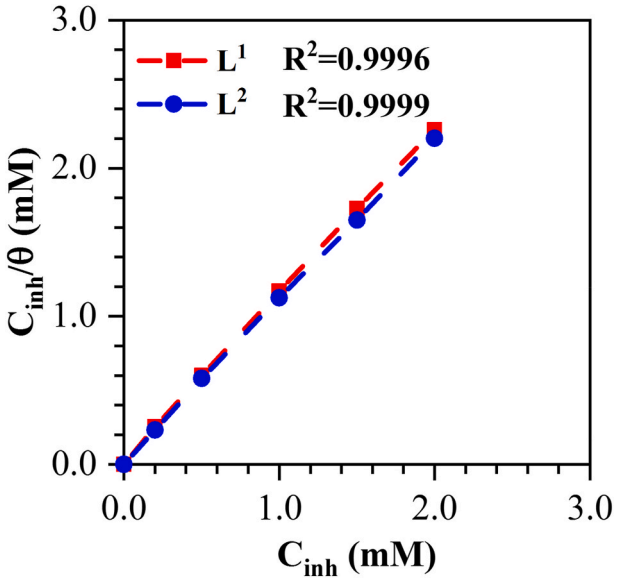

Fig. 9. Langmuir adsorption isotherms involving L^1 and its reduced form (L^2).

Fig. 8 shows the EDS profile analyses of as-received C-steel before dipping in the electrolyte, the sample immersed in 1.0 M HCl, 2.0 mM L^1 and the L^2-containing solutions. The EDS profile obtained on the C-steel surface illustrates that the main peak is iron and carbon, representing the steel composition. The surface of the C-steel immersed in the 1.0 M HCl shows one more peak, which corresponds to oxygen. The additional peak owing to oxygen indicates the formation of the steel corrosion product on the surface. The EDS spectrum of C-steel exposed in the 1.0 HCl solutions in the presence of 2.0 mM L^1 and L^2 do not demonstrate the oxygen peak, implying the protective layer of inhibitors on the C-steel surface. The results confirmed that the addition of L^1 and L^2 in 1.0 M HCl effectively hinders the corrosion of the C-steel.

3.6. Adsorption mechanism

The adsorption of inhibitors on the surface of the C-steel electrode is the vital step in an inhibition mechanism [17]. The main reason for higher corrosion protection in the presence of inhibitors is the adsorption of this material on the C-steel surface. Based on the previous studies [15,39], the Langmuir adsorption model is the best model to explain the adsorption process of the inhibitors of L^1 and L^2 on the surface of C-steel in 1.0 M HCl. The Langmuir adsorption isotherm, which is based on a simple kinetic model for monolayer adsorption on the surface, is presented as follows:

$$\frac{C_{inh}}{\theta} = \frac{1}{K_{ads}} + C_{inh} \tag{6}$$

where K_{ads} the adsorption equilibrium constant, C_{inh} is the concentration of inhibitor, and θ is the fraction of surface coverage by the inhibitor molecule, which is calculated by the following equation [38]:

$$\theta = 1 - \frac{C_{dl}^{i}}{C_{dl}^{b}} \tag{7}$$

where C_{dl}^{i} is the capacitive response of the carbon steel electrode resulting in the inhibitor-containing and C_{dl}^{b} is capacitive of the double layer in the free-inhibitor solution. Langmuir relationship, a plot of C_{inh}/θ against C_{inh} should yield a straight line via the regression coefficient, R^2 (shown in Fig. 9). The R^2 values give a good agreement between the EIS and Langmuir data for L^1 (R^2 = 0.9996) and L^2 (R^2 = 0.9999) inhibitors. The near-unity slope for L^1 and L^2-containing solutions (i.e., slope = 1.12 and 1.05, respectively) supports the suitability of the

Table 7
The calculated quantum chemical parameters of inhibitors.

	E_{HOMO}	E_{LUMO}	I	A	ΔE	η	Σ	X	Pİ	ω	ε	dipol	Energy
B3LYP/6–31+g LEVEL													
1	−5,4274	−0,8675	5,4274	0,8675	4,5598	2,2799	0,4386	3,1474	−3,1474	2,1725	0,4603	4,7422	−41884,5606
2	−5,2581	−0,5018	5,2581	0,5018	4,7563	2,3782	0,4205	2,8799	−2,8799	1,7438	0,5735	4,0596	−41917,1468
HF/6–31+g LEVEL													
1	−8,0642	2,5987	8,0642	−2,5987	10,6629	5,3314	0,1876	2,7327	−2,7327	0,7004	1,4278	2,4128	−41605,3465
2	−8,2315	3,5144	8,2315	−3,5144	11,7459	5,8729	0,1703	2,3586	−2,3586	0,4736	2,1115	4,1761	−41636,1458
M062X/6–31+g LEVEL													
1	−7,0269	0,1039	7,0269	−0,1039	7,1308	3,5654	0,2805	3,4615	−3,4615	1,6803	0,5951	4,4003	−41866,4346
2	−6,9373	0,5382	6,9373	−0,5382	7,4756	3,7378	0,2675	3,1995	−3,1995	1,3694	0,7302	3,8441	−41899,0131

Table 8
The calculated quantum chemical parameters of inhibitors.

	E_{HOMO}	E_{LUMO}	I	A	ΔE	η	Σ	X	Pİ	ω	ε	dipol	Energy
B3LYP/6–31++g LEVEL													
1	−5,7193	−1,1875	5,7193	1,1875	4,5318	2,2659	0,4413	3,4534	−3,4534	2,6316	0,3800	4,9934	−41886,1091
2	−5,5803	−0,9121	5,5803	0,9121	4,6681	2,3341	0,4284	3,2462	−3,2462	2,2574	0,4430	4,0488	−41918,7373
HF/6–31++g LEVEL													
1	−8,6508	0,8934	8,6508	−0,8934	9,5442	4,7721	0,2096	3,8787	−3,8787	1,5763	0,6344	2,8098	−41605,9430
2	−8,3850	0,8906	8,3850	−0,8906	9,2756	4,6378	0,2156	3,7472	−3,7472	1,5138	0,6606	4,1414	−41637,1374
M062X/6–31++g LEVEL													
1	−7,2459	−0,2634	7,2459	0,2634	6,9825	3,4912	0,2864	3,7547	−3,7547	2,0190	0,4953	4,5038	−41867,6736
2	−7,1863	−0,4338	7,1863	0,4338	6,7526	3,3763	0,2962	3,8100	−3,8100	2,1498	0,4652	3,7428	−41900,3243

Table 9
The calculated quantum chemical parameters of inhibitors.

	E_{HOMO}	E_{LUMO}	I	A	ΔE	η	Σ	X	Pİ	ω	ε	dipol	Energy
B3LYP/6–31++g (d,p) LEVEL													
1	−5,9373	−1,1712	5,9373	1,1712	4,7661	2,3831	0,4196	3,5542	−3,5542	2,6505	0,3773	4,4151	−41899,6892
2	−5,8804	−0,8955	5,8804	0,8955	4,9849	2,4924	0,4012	3,3880	−3,3880	2,3026	0,4343	3,7854	−41932,2514
HF/6–31++g (d,p) LEVEL													
1	−8,0848	0,9802	8,0848	−0,9802	9,0650	4,5325	0,2206	3,5523	−3,5523	1,3921	0,7184	4,3616	−41625,4290
2	−8,1970	0,8985	8,1970	−0,8985	9,0955	4,5477	0,2199	3,6492	−3,6492	1,4641	0,6830	3,7140	−41656,8335
M062X/6–31++g (d,p) LEVEL													
1	−7,2369	−0,2465	7,2369	0,2465	6,9904	3,4952	0,2861	3,7417	−3,7417	2,0028	0,4993	3,9070	−41880,3065
2	−7,3063	−0,4240	7,3063	0,4240	6,8824	3,4412	0,2906	3,8651	−3,8651	2,1707	0,4607	3,5402	−41912,8041

Table 10
The calculated quantum chemical parameters of inhibitors.

	E_{HOMO}	E_{LUMO}	I	A	ΔE	η	Σ	X	Pİ	ω	ε	dipol	Energy
B3LYP/6–31+g LEVEL													
1	−6,9420	−4,8219	6,9420	4,8219	2,1201	1,0600	0,9434	5,8819	−5,8819	16,3189	0,0613	33,5474	−41893,5312
2	−7,0315	−4,4850	7,0315	4,4850	2,5465	1,2732	0,7854	5,7582	−5,7582	13,0210	0,0768	23,9338	−41925,5171
HF/6–31+g LEVEL													
1	−9,4147	−0,0038	9,4147	0,0038	9,4109	4,7054	0,2125	4,7092	−4,7092	2,3565	0,4244	29,0210	−41614,2315
2	−11,0906	0,1951	11,0906	−0,1951	11,2857	5,6429	0,1772	5,4478	−5,4478	2,6297	0,3803	13,4799	−41646,8833
M062X/6–31+g LEVEL													
1	−8,3044	−3,5122	8,3044	3,5122	4,7922	2,3961	0,4173	5,9083	−5,9083	7,2843	0,1373	33,7350	−41875,1812
2	−8,7749	−3,3696	8,7749	3,3696	5,4053	2,7027	0,3700	6,0723	−6,0723	6,8215	0,1466	22,7482	−41907,2417

Table 11
The calculated quantum chemical parameters of inhibitors.

	E_{HOMO}	E_{LUMO}	I	A	ΔE	η	Σ	X	Pİ	ω	ε	dipol	Energy
B3LYP/6–31++g LEVEL													
1	−7,2070	−5,3196	7,2070	5,3196	1,8874	0,9437	1,0597	6,2633	−6,2633	20,7846	0,0481	33,3897	−41894,9229
2	−7,3558	−5,1041	7,3558	5,1041	2,2518	1,1259	0,8882	6,2300	−6,2300	17,2365	0,0580	23,3850	−41926,9453
HF/6–31++g LEVEL													
1	−9,4049	−2,4265	9,4049	2,4265	6,9784	3,4892	0,2866	5,9157	−5,9157	5,0148	0,1994	33,2438	−41614,6495
2	−11,2218	−1,8956	11,2218	1,8956	9,3262	4,6631	0,2144	6,5587	−6,5587	4,6124	0,2168	13,2422	−41647,7705
M062X/6–31++g LEVEL													
1	−8,5096	−4,4679	8,5096	4,4679	4,0417	2,0209	0,4948	6,4887	−6,4887	10,4172	0,0960	33,7687	−41876,4072
2	−9,4705	−3,4986	9,4705	3,4986	5,9719	2,9859	0,3349	6,4845	−6,4845	7,0412	0,1420	12,1952	−41910,7910

Table 12
The calculated quantum chemical parameters of inhibitors.

	E_{HOMO}	E_{LUMO}	I	A	ΔE	η	Σ	X	Pİ	ω	ε	dipol	Energy
B3LYP/6–31++g (d,p) LEVEL													
1	−7,1898	−5,0959	7,1898	5,0959	2,0939	1,0470	0,9551	6,1429	−6,1429	18,0211	0,0555	31,9798	−41908,3685
2	−7,3558	−5,1041	7,3558	5,1041	2,2518	1,1259	0,8882	6,2300	−6,2300	17,2365	0,0580	23,3850	−41926,9453
HF/6–31++g (d,p) LEVEL													
1	−9,3009	−2,4561	9,3009	2,4561	6,8448	3,4224	0,2922	5,8785	−5,8785	5,0486	0,1981	32,8781	−41634,2688
2	−10,5687	−2,3620	10,5687	2,3620	8,2067	4,1034	0,2437	6,4653	−6,4653	5,0934	0,1963	22,4671	−41665,0021
M062X/6–31++g (d,p) LEVEL													
1	−8,4892	−4,2970	8,4892	4,2970	4,1922	2,0961	0,4771	6,3931	−6,3931	9,7494	0,1026	32,1212	−41888,8771
2	−9,5129	−2,5783	9,5129	2,5783	6,9346	3,4673	0,2884	6,0456	−6,0456	5,2706	0,1897	11,2549	−41930,2612

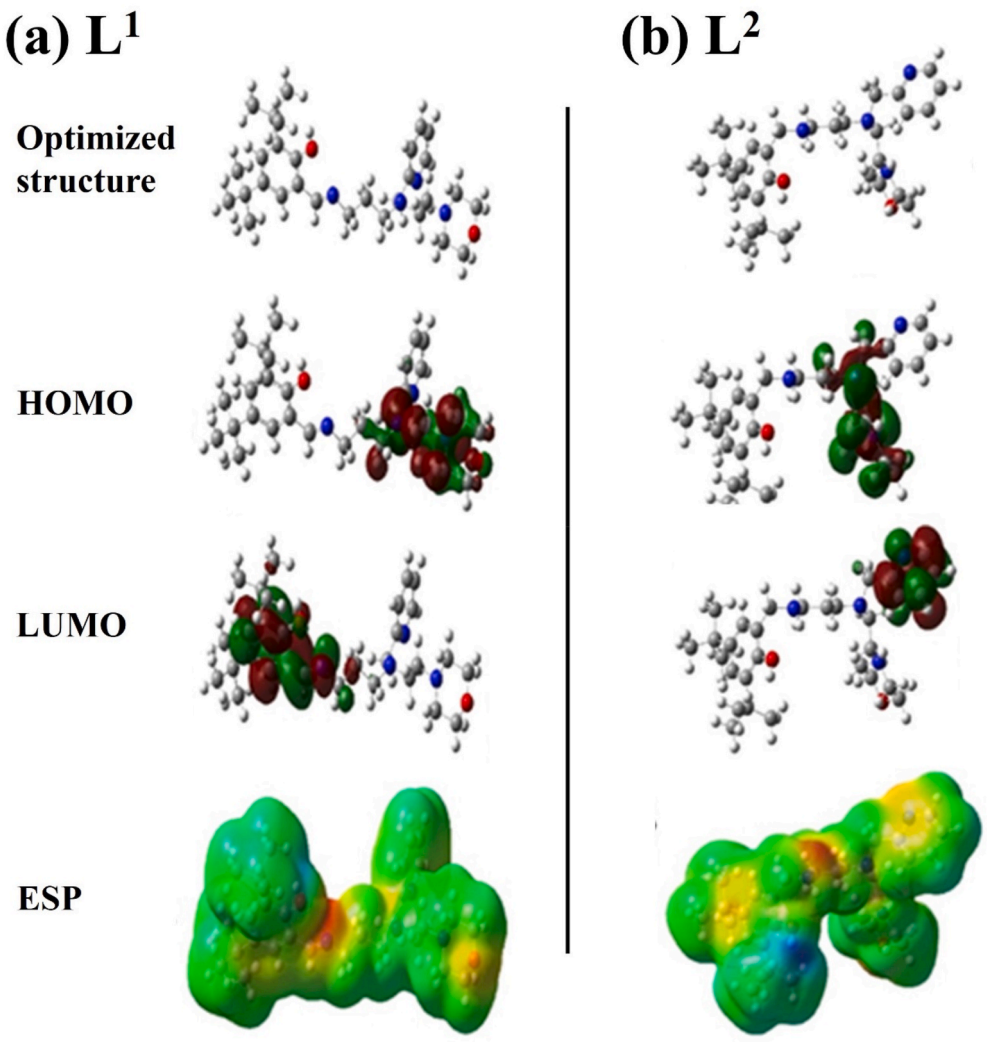

Fig. 10. Representations of optimized structures, HOMO, LUMO, and ESP shapes of inhibitor molecules.

Langmuir model for obtained results in the present study.

The value of K_{ads} can be calculated by considering the width of the original value of the C_{inh}/θ against C_{inh} diagrams. The K_{ads} obtained for L^1 and L^2 inhibitors are 49.26 and 102.04 $(mM)^{-1}$, respectively. The Langmuir K_{ads} value can be interpreted as the adsorption/desorption equilibrium for each inhibitor on the surface of the C-steel. In other words, it describes the fraction of the electrode surface, which is covered by inhibitor molecules. The higher the adsorption equilibrium constant, the more corrosion protection there appears to be.

3.7. Theoretical studies

Today, the use of theoretical approaches to compare inhibitor molecules has become widespread. However, in the calculations made by theoretical methods, many quantum chemical parameters about inhibitor molecules are obtained. These quantum chemical parameters enable us to gain information faster than experimental methods to explain the inhibitory properties of inhibitor molecules. Among these quantum chemical parameters, the two most important parameters are HOMO and LUMO. The HOMO parameter of the molecule shows the ability of inhibitor molecules to donate electrons from the highest energy-filled orbitals to metal atoms.

On the other hand, the LUMO parameter of molecules indicates the ability of molecules to receive electrons from metal atoms to the lowest energy empty molecular orbitals. These two parameters either create a chemical interaction by giving electrons from metal atoms to inhibitor molecules for the molecules to hold onto the metal surface, or make a chemical interaction by donating electrons to metal atoms from inhibitor molecules. The numerical values of all calculated parameters with various basis sets are given in Tables 7–12.

The calculations of the molecules were made in different methods and basis sets. Calculations of 6–31+g, 6–31++g, and 6–31++g(d,p) basis sets were made in this method and basis sets B3LYP, HF, M062X method. In these calculations, many quantum chemical parameters of the molecules are calculated. After the heteroatoms in the molecule were examined, the nitrogen atom with the most negative charge was protonated. In experimental processes, the acid molecule in solution causes the protonation of this most negatively charged heteroatom. For this reason, calculations of the protonated states of the molecules were made. As a result of the calculations, it was seen that the inhibitory activity of L^2 was higher than that of L^1.

Although many parameters are obtained in the calculations, there is a formal demonstration of the two parameters. The first picture in Fig. 10 shows the optimized structures of the inhibitor molecules. In the second and third pictures, there are HOMO and LUMO representations of the inhibitor molecules. The last picture shows which atoms in inhibitor molecules have greater electron density [52].

HOMO and LUMO parameters of molecules are calculated with theoretical calculations. With these calculations, it is possible to comment on the electron exchanges and inhibitory activities of molecules. However, in ESP shapes of molecules, the red colored regions of the molecules are electron-rich regions. The blue colored regions are electron-poor regions. The electron-rich regions of the molecules allow the molecules to show inhibitory activity by donating electrons. However, the electron-poor regions of the molecules allow the molecules to accept electrons and show inhibitory activity. The ESP results of the molecules with the calculations made the nitrogen atom in the center of the L^1 molecule and the oxygen atoms at the end of the molecule are shown in red. These regions are electron-rich regions. On the other hand, it is seen that the same atoms in the L^2 molecule are colored red. In general, the blue colored regions are on the methyl groups attached to the benzene ring. Since the methyl group is not able to accept electrons, it is believed that the inhibitory mechanism will proceed through the red colored regions. Since the methyl group is not able to accept electrons, it is thought that the inhibitory mechanism will proceed through the red colored regions. This situation shows heteroatoms in molecules, that is, atoms such as oxygen, nitrogen, and sulfur, other than carbon atoms in organic and inorganic compounds. They show inhibitory activity by donating lone electron pairs on these atoms.

4. Conclusion

The corrosion behavior of C-steel in 1.0 M HCl with and without inhibitors was investigated using electrochemical techniques. The main conclusions of the present study are summarized below:

1. From Tafel's results, the highest value of i_{corr} corresponded to the inhibitor-free solution, suggesting a higher corrosion rate than other inhibitor-containing solutions.
2. The i_{corr} for C-steel in the L^1-containing solution decreases gradually by raising the concentration of L^1 from 0.2 to 2.0 mM. It is seen that the addition of a reduced form of L^1 in the 1.0 M HCl solution provided a superior result with the best resistance to corrosion as compared to the L^1-free and containing solutions.
3. The addition of L^1 and L^2 inhibitors to the 1.0 M HCl electrolyte decreases the corrosion rate of steel in the electrolyte. The compound L^2 was found to show a better inhibitor characteristic than L^1 due to the higher stability in HCl solution.
4. The result showed that the inhibition efficiency of L^2 enhances with increasing the concentration and presented the highest value at a concentration of 2.0 mM (e.g., 90.86%). The same trend can be found in the L^1-containing solution, in which the corrosion rate of the C-steel tends to decrease by an increment of L^1 and presented a minimum rate at 2.0 mM in the range of 0.1–2.0 mM.
5. SEM images supported the protection of inhibitors against the corrosion of the C-steel surface in 1.0 M HCl solution.
6. Both adsorption of L^1 and its reduced form on the surface of the C-steel followed the Langmuir adsorption isotherm.
7. As a result of the theoretical calculations, many quantum chemical parameters have been obtained. Each parameter obtained provides important information about the inhibitory properties of inhibitor molecules. The numerical values of the parameters obtained indicate that the L^2 inhibitor molecule is better than the other.

CRediT authorship contribution statement

Saeid Karimi: Data curation, Methodology, Writing – review & editing. **Majid Rezaeivala:** Conceptualization, Writing – review & editing. **Koray Sayin:** Software, Investigation, Validation. **Burak Tuzun:** Software.

Declaration of competing interest

The authors declare that they have no known competing financial interests or personal relationships that could have appeared to influence the work reported in this paper.

Acknowledgment

We thank the Hamedan University of Technology for financial support. Also, this work was supported by the Research Fund of TÜBİTAK ULAKBİM High Performance and Grid Computing Center (TR-Grid e-Infrastructure).

References

[1] I. Ahamad, R. Prasad, M.A. Quraishi, Thermodynamic, electrochemical and quantum chemical investigation of some Schiff bases as corrosion inhibitors for mild steel in hydrochloric acid solutions, Corrosion Sci. 52 (2010) 933–942, https://doi.org/10.1016/j.corsci.2009.11.016.

[2] Y. Luo, M. Bernien, A. Krüger, C.F. Hermanns, J. Miguel, Y.M. Chang, S. Jaekel, W. Kuch, R. Haag, In situ hydrolysis of imine derivatives on Au(111) for the formation of aromatic mixed self-assembled monolayers: multitechnique analysis of this tunable surface modification, Langmuir 28 (2012) 358–366, https://doi.org/10.1021/la202696a.

[3] M. Rezaeivala, H. Keypour, Schiff base and non-Schiff base macrocyclic ligands and complexes incorporating the pyridine moiety - the first 50 years, Coord. Chem. Rev. 280 (2014) 203–253, https://doi.org/10.1016/j.ccr.2014.06.007.

[4] H. Keypour, M. Rezaeivala, L. Valencia, P. Pérez-Lourido, H.R. Khavasi, Synthesis and characterization of some new Co(II) and Cd(II) macroacyclic Schiff-base complexes containing piperazine moiety, Polyhedron 28 (2009) 4096–4100, https://doi.org/10.1016/j.poly.2009.09.031.

[5] H. Keypour, M. Rezaeivala, M. Mirzaei-Monsef, K. Sayin, N. Dilek, H. Unver, Synthesis and characterization of Co(II), Ni(II), Cu(II) and Zn(II) complexes with a new homopiperazine macrocyclic Schiff base ligand, Inorg. Chim. Acta. 432 (2015) 243–249, https://doi.org/10.1016/j.ica.2015.04.017.

[6] M. Rezaeivala, M. Ahmadi, B. Captain, S. Şahin-Bölükbaşı, A.A. Dehghani-Firouzabadi, R. William Gable, Synthesis, characterization, and cytotoxic activity studies of new N4O complexes derived from 2-({3-[2-morpholinoethylamino]-N3-([pyridine-2-yl]methyl) propylimino} methyl)phenol, Appl. Organomet. Chem. 34 (2020), e5325, https://doi.org/10.1002/aoc.5325.

[7] M. Rezaeivala, M. Ahmadi, B. Captain, M. Bayat, M. Saeidirad, S. Şahin-Bölükbaşı, B. Yıldız, R.W. Gable, Some new morpholine-based Schiff-base complexes; Synthesis, characterization, anticancer activities and theoretical studies, Inorg. Chim. Acta. 513 (2020), 119935, https://doi.org/10.1016/j.ica.2020.119935.

[8] B. Chugh, A.K. Singh, S. Thakur, B. Pani, H. Lgaz, I.M. Chung, R. Jha, E.E. Ebenso, Comparative investigation of corrosion-mitigating behavior of thiadiazole-derived bis-schiff bases for mild steel in acid medium: experimental, theoretical, and surface study, ACS Omega 5 (2020) 13503–13520, https://doi.org/10.1021/acsomega.9b04274.

[9] B.A. Ismail, D.A. Nassar, Z.H. Abd El–Wahab, O.A.M. Ali, Synthesis, characterization, thermal, DFT computational studies and anticancer activity of

furfural-type schiff base complexes, J. Mol. Struct. 1227 (2021), 129393, https://doi.org/10.1016/j.molstruc.2020.129393.
[10] G. Kılınççeker, S. Çelik, F. Zarifi, K. Sayın, Experimental and computational investigation of variamine blue as an inhibitor for copper in chloride solution, J. Dispersion Sci. Technol. (2020) 1–7, https://doi.org/10.1080/01932691.2020.1845194.
[11] M. Murmu, S.K. Saha, N.C. Murmu, P. Banerjee, Effect of stereochemical conformation into the corrosion inhibitive behaviour of double azomethine based Schiff bases on mild steel surface in 1 mol L−1 HCl medium: an experimental, density functional theory and molecular dynamics simulation study, Corrosion Sci. 146 (2019) 134–151, https://doi.org/10.1016/j.corsci.2018.10.002.
[12] L.O. Olasunkanmi, E.E. Ebenso, Experimental and computational studies on propanone derivatives of quinoxalin-6-yl-4,5-dihydropyrazole as inhibitors of mild steel corrosion in hydrochloric acid, J. Colloid Interface Sci. 561 (2020) 104–116, https://doi.org/10.1016/j.jcis.2019.11.097.
[13] H. Jafari, K. Sayin, Sulfur containing compounds as corrosion inhibitors for mild steel in hydrochloric acid solution, Trans. Indian Inst. Met. 69 (2016) 805–815, https://doi.org/10.1007/s12666-015-0556-2.
[14] A. Singh, K.R. Ansari, D.S. Chauhan, M.A. Quraishi, H. Lgaz, I.M. Chung, Comprehensive investigation of steel corrosion inhibition at macro/micro level by ecofriendly green corrosion inhibitor in 15% HCl medium, J. Colloid Interface Sci. 560 (2020) 225–236, https://doi.org/10.1016/j.jcis.2019.10.040.
[15] A.B. da Silva, E. D'Elia, J.A. da Cunha Ponciano Gomes, Carbon steel corrosion inhibition in hydrochloric acid solution using a reduced Schiff base of ethylenediamine, Corrosion Sci. 52 (2010) 788–793, https://doi.org/10.1016/j.corsci.2009.10.038.
[16] R. Rihan, R. Shawabkeh, N. Al-Bakr, The effect of two amine-based corrosion inhibitors in improving the corrosion resistance of carbon steel in sea water, J. Mater. Eng. Perform. 23 (2014) 693–699, https://doi.org/10.1007/s11665-013-0790-x.
[17] H. Jafari, F. mohsenifar, K. Sayin, Corrosion inhibition studies of N,N'-bis(4-formylphenol)-1,2-Diaminocyclohexane on steel in 1 HCl solution acid, J. Taiwan Inst. Chem. Eng. 64 (2016) 314–324, https://doi.org/10.1016/j.jtice.2016.04.021.
[18] E.A. Badr, M.A. Bedair, S.M. Shaban, Adsorption and performance assessment of some imine derivatives as mild steel corrosion inhibitors in 1.0 M HCl solution by chemical, electrochemical and computational methods, Mater. Chem. Phys. 219 (2018) 444–460, https://doi.org/10.1016/j.matchemphys.2018.08.041.
[19] L.O. Olasunkanmi, M.F. Sebona, E.E. Ebenso, Influence of 6-phenyl-3(2H)-pyridazinone and 3-chloro-6-phenylpyrazine on mild steel corrosion in 0.5 M HCl medium: experimental and theoretical studies, J. Mol. Struct. 1149 (2017) 549–559, https://doi.org/10.1016/j.molstruc.2017.08.018.
[20] H.M. Abd El-Lateef, K. Shalabi, A.H. Tantawy, Corrosion inhibition and adsorption features of novel bioactive cationic surfactants bearing benzenesulphonamide on C1018-steel under sweet conditions: combined modeling and experimental approaches, J. Mol. Liq. 320 (2020), 114564, https://doi.org/10.1016/j.molliq.2020.114564.
[21] A. Kosari, M.H. Moayed, A. Davoodi, R. Parvizi, M. Momeni, H. Eshghi, H. Moradi, Electrochemical and quantum chemical assessment of two organic compounds from pyridine derivatives as corrosion inhibitors for mild steel in HCl solution under stagnant condition and hydrodynamic flow, Corrosion Sci. 78 (2014) 138–150, https://doi.org/10.1016/j.corsci.2013.09.009.
[22] A.L. de Q. Baddini, S.P. Cardoso, E. Hollauer, J.A. da C.P. Gomes, Statistical analysis of a corrosion inhibitor family on three steel surfaces (duplex, super-13 and carbon) in hydrochloric acid solutions, Electrochim. Acta 53 (2007) 434–446, https://doi.org/10.1016/j.electacta.2007.06.050.
[23] Z. Tang, A review of corrosion inhibitors for rust preventative fluids, Curr. Opin. Solid State Mater. Sci. 23 (2019), 100759, https://doi.org/10.1016/j.cossms.2019.06.003.
[24] E. Barmatov, T. Hughes, Degradation of a schiff-base corrosion inhibitor by hydrolysis, and its effects on the inhibition efficiency for steel in hydrochloric acid, Mater. Chem. Phys. 257 (2021), 123758, https://doi.org/10.1016/j.matchemphys.2020.123758.
[25] K.C. Emregül, O. Atakol, Corrosion inhibition of iron in 1 M HCl solution with Schiff base compounds and derivatives, Mater. Chem. Phys. 83 (2004) 373–379, https://doi.org/10.1016/j.matchemphys.2003.11.008.
[26] K.M. Emran, N.M. Ahmed, B.A. Torjoman, A.A. Al-Ahmadi, S.N. Sheekh, Cantaloupe extracts as eco friendly corrosion inhibitors for aluminum in acidic and alkaline solutions, J. Mater. Environ. Sci. 5 (2014) 1940–1950.
[27] M. Rezaeivala, H. Keypour, S. Salehzadeh, R. Latifi, F. Chalabian, F. Katouzian, Synthesis, characterization and crystal structure of some new Mn(II) and Zn(II) macroacyclic Schiff base complexes derived from two new asymmetrical (N5) branched amines and pyridine-2-carbaldehyde or O-vaniline and their antibacterial properties, J. Iran. Chem. Soc. 11 (2014) 431–440, https://doi.org/10.1007/s13738-013-0315-4.
[28] H. Keypour, M. Shayesteh, A. Sharifi-Rad, S. Salehzadeh, H. Khavasi, L. Valencia, Synthesis and characterization of copper(II) and cobalt(II) complexes with two new potentially hexadentate Schiff base ligands. X-ray crystal structure determination of one copper(II) complex, J. Organomet. Chem. 693 (2008) 3179–3187, https://doi.org/10.1016/j.jorganchem.2008.07.012.
[29] F.D.J. Frisch M J, G.W. Trucks, H.B. Schlegel, G.E. Scuseria, M.A. Robb, J. R. Cheeseman, G. Scalmani, V. Barone, B. Mennucci, G.A. Petersson, H. Nakatsuji, M. Caricato, X. Li, H.P. Hratchian, A.F. Izmaylov, J. Bloino, G. Zheng, J. L. Sonnenberg, M. Hada, M. Ehara, Gaussian 09, Rev. D. 01, Gaussian Inc., Wallingford CT, 2009.
[30] A. Üngördü, N. Tezer, The solvent (water) and metal effects on HOMO-LUMO gaps of guanine base pair: a computational study, J. Mol. Graph. Model. 74 (2017) 265–272, https://doi.org/10.1016/j.jmgm.2017.04.015.
[31] N.R. Sheela, S. Muthu, S. Sampathkrishnan, Molecular orbital studies (hardness, chemical potential and electrophilicity), vibrational investigation and theoretical NBO analysis of 4-4′-(1H-1,2,4-triazol-1-yl methylene) dibenzonitrile based on abinitio and DFT methods, Spectrochim. Acta Part A Mol. Biomol. Spectrosc. 120 (2014) 237–251, https://doi.org/10.1016/j.saa.2013.10.007.
[32] A. Heidarpour, Z.S. Mousavi, S. Karimi, S.M. Hosseini, On the corrosion behavior and microstructural characterization of Al2024 and Al2024/Ti_2SC MAX phase surface composite through friction stir processings, J. Appl. Electrochem. (2021) 1–14, https://doi.org/10.1007/s10800-021-01567-9.
[33] L. Fang, L. Xie, J. Hu, Y. Li, W. Zhang, Study on the growth and corrosion resistance of manganese phosphate coatings on 30CrMnMoTi alloy steel, Phys. Procedia 18 (2011) 227–233, https://doi.org/10.1016/j.phpro.2011.06.086.
[34] K. Wan, P. Feng, B. Hou, Y. Li, Enhanced corrosion inhibition properties of carboxymethyl hydroxypropyl chitosan for mild steel in 1.0 M HCl solution, RSC Adv. 6 (2016) 77515–77524, https://doi.org/10.1039/c6ra12975g.
[35] H.H. Hassan, E. Abdelghani, M.A. Amin, Inhibition of mild steel corrosion in hydrochloric acid solution by triazole derivatives. Part I. Polarization and EIS studies, Electrochim. Acta 52 (2007) 6359–6366, https://doi.org/10.1016/j.electacta.2007.04.046.
[36] F.S. de Souza, A. Spinelli, Caffeic acid as a green corrosion inhibitor for mild steel, Corrosion Sci. 51 (2009) 642–649, https://doi.org/10.1016/j.corsci.2008.12.013.
[37] M. Faiz, A. Zahari, K. Awang, H. Hussin, Corrosion inhibition on mild steel in 1 M HCl solution by: Cryptocarya nigra extracts and three of its constituents (alkaloids), RSC Adv. 10 (2020) 6547–6562, https://doi.org/10.1039/c9ra05654h.
[38] M. Rezaeivala, S. Karimi, B. Tuzun, K. Sayin, Anti-corrosion behavior of 2-((3-(2-morpholino ethylamino) -N3-((pyridine-2-yl)methyl)propylimino)methyl)pyridine and its reduced form on Carbon Steel in Hydrochloric Acid solution: experimental and theoretical studies, Thin Solid Films 741 (2022), 139036, https://doi.org/10.1016/j.tsf.2021.139036.
[39] S. Satpati, S.K. Saha, A. Suhasaria, P. Banerjee, D. Sukul, Adsorption and anti-corrosion characteristics of vanillin Schiff bases on mild steel in 1 M HCl: experimental and theoretical study, RSC Adv. 10 (2020) 9258–9273, https://doi.org/10.1039/c9ra07982c.
[40] L. Li, M. Soleymani, A. Ghahreman, New insights on the role of lattice-substituted silver in catalytic oxidation of chalcopyrite, Electrochim. Acta 369 (2021), 137652, https://doi.org/10.1016/j.electacta.2020.137652.
[41] N.Z.N. Hashim, M.A.M. Kahar, K. Kassim, Z. Embong, E.H. Anouar, Experimental and theoretical studies of azomethines derived from benzylamine as corrosion inhibitors of mild steel in 1 M HCl, J. Mol. Struct. 1222 (2020), 128899, https://doi.org/10.1016/j.molstruc.2020.128899.
[42] J.K. Odusote, T.B. Asafa, J.G. Oseni, A.A. Adeleke, A.A. Adediran, R.A. Yahya, J. M. Abdul, S.A. Adedayo, Inhibition efficiency of gold nanoparticles on corrosion of mild steel, stainless steel and aluminium in 1M HCl solution, Mater. Today Proc. 38 (2021) 578–583, https://doi.org/10.1016/j.matpr.2020.02.984.
[43] W. Chen, B. Nie, M. Liu, H.J. Li, D.Y. Wang, W. Zhang, Y.C. Wu, Mitigation effect of quinazolin-4(3H)-one derivatives on the corrosion behaviour of mild steel in HCl, Colloids Surfaces A Physicochem. Eng. Asp. 627 (2021), 127188, https://doi.org/10.1016/j.colsurfa.2021.127188.
[44] E.E. Elemike, H.U. Nwankwo, D.C. Onwudiwe, Synthesis and comparative study on the anti-corrosion potentials of some Schiff base compounds bearing similar backbone, J. Mol. Liq. 276 (2019) 233–242, https://doi.org/10.1016/j.molliq.2018.11.161.
[45] K. Vimal, R.B.V. Appa, Chemically modified biopolymer as an eco-friendly corrosion inhibitor for mild steel in a neutral chloride environment, New J. Chem. 41 (2017) 6278–6289, https://doi.org/10.1039/c7nj00553a.
[46] H. Ashassi-Sorkhabi, Z. Ghasemi, D. Seifzadeh, The inhibition effect of some amino acids towards the corrosion of aluminum in 1 M HCl + 1 M H 2 SO 4 solution, Appl. Surf. Sci. 249 (2005) 408–418, https://doi.org/10.1016/j.apsusc.2004.12.016.
[47] S. Karimi, A. Ghahreman, F. Rashchi, J. Moghaddam, The mechanism of electrochemical dissolution of sphalerite in sulfuric acid media, Electrochim. Acta 253 (2017) 47–58, https://doi.org/10.1016/j.electacta.2017.09.040.
[48] I.A.W. Ma, S. Ammar, S.S.A. Kumar, K. Ramesh, S. Ramesh, A concise review on corrosion inhibitors: types, mechanisms and electrochemical evaluation studies, J. Coating Technol. Res. 19 (2022) 241–268, https://doi.org/10.1007/s11998-021-00547-0.
[49] S. Chakri, I. Frateur, M.E. Orazem, E.M.M. Sutter, T.T.M. Tran, B. Tribollet, V. Vivier, Improved EIS analysis of the electrochemical behaviour of carbon steel in alkaline solution, Electrochim. Acta 246 (2017) 924–930, https://doi.org/10.1016/j.electacta.2017.06.096.
[50] N. Attarzadeh, K. Raeissi, M.A. Golozar, Effect of saccharin addition on the corrosion resistance of polypyrrole coatings, Prog. Org. Coating 63 (2008) 167–174, https://doi.org/10.1016/j.porgcoat.2008.05.005.
[51] P.E. Alvarez, M.V. Fiori-Bimbi, A. Neske, S.A. Brandán, C.A. Gervasi, Rollinia occidentalis extract as green corrosion inhibitor for carbon steel in HCl solution, J. Ind. Eng. Chem. 58 (2018) 92–99, https://doi.org/10.1016/j.jiec.2017.09.012.
[52] A.M. Bayoumy, M. Ibrahim, A. Omar, Mapping molecular electrostatic potential (MESP) for fulleropyrrolidine and its derivatives, Opt. Quant. Electron. 52 (2020) 1–13, https://doi.org/10.1007/s11082-020-02467-6.